Communication
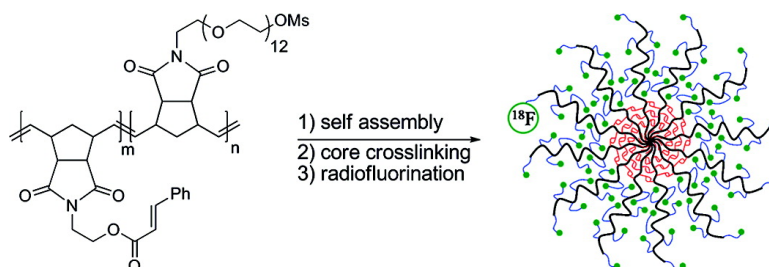
Synthesis of Fluorine-18 Functionalized Nanoparticles for use as in vivo Molecular Imaging Agents

John B. Matson, and Robert H. Grubbs

More About This Article

Additional resources and features associated with this article are available within the HTML version:

- Supporting Information
- Links to the 1 articles that cite this article, as of the time of this article download
- Access to high resolution figures
- Links to articles and content related to this article
- Copyright permission to reproduce figures and/or text from this article

View the Full Text HTML

Synthesis of Fluorine-18 Functionalized Nanoparticles for use as in vivo Molecular Imaging Agents

John B. Matson and Robert H. Grubbs*

NanoSystems Biology Cancer Center, Division of Chemistry and Chemical Engineering, MC 127-72, California Institute of Technology, Pasadena, California 91125

Received March 18, 2008; E-mail: rhg@caltech.edu

Nanostructures are the subject of intense study toward applications in cancer diagnosis, imaging, and treatment.[1] Research in this area is driven by the observation that particles in the nanometer size range are known to localize more heavily in tumor tissue than in healthy tissue. This phenomenon, known as the enhanced permeability and retention effect (EPR effect), is due to the leaky vasculature exhibited in the tumor tissue.[2] Exploitation of the EPR effect is a common strategy for targeting tumor cells, using nanostructures including liposomes,[3] quantum dots,[4] dendrimers,[5] polymeric micelles,[6] and other molecular conjugates.[7]

Imaging of nanostructures designed to detect tumors by exploiting the EPR effect has been accomplished using several in vivo imaging techniques, including magnetic resonance (MR),[8] near-IR fluorescence (NIR),[9] and positron emission tomography (PET).[10] Of these techniques, PET is the most sensitive and accurate method of measuring the temporal pattern in the biodistribution of nanoparticles as PET is a specific, highly sensitive, and versatile three-dimensional molecular imaging technique that is used broadly in tumor imaging. The most widespread radionuclide used in PET imaging is fluorine-18, which is the positron-emitting isotope in the commonly used PET tracer 18-fluorodeoxyglucose. Due to its relatively long half-life ($t_{1/2}$ = 109 min), many more fluorine-18-containing radiotracers are synthetically accessible than are radiotracers with other small positron-emitting nuclides, such as carbon-11 ($t_{1/2}$ = 20 min), nitrogen-13 ($t_{1/2}$ = 10 min), and oxygen-15 ($t_{1/2}$ = 2 min). This has led to a dramatic increase in recent years in the production of fluorine-18, which can only be synthesized in a cyclotron.

To our knowledge, no reports of tumor-targeting nanoparticles functionalized with fluorine-18 have been published. While nanoparticles incorporating positron-emitting metals such as copper-64 ($t_{1/2}$ = 12.7 h)[10a–c] have been synthesized, rapid and efficient incorporation of fluorine-18 into nanoparticles remains elusive. Incorporation of this common PET nuclide into nanoparticles would pave the way for precise and accurate in vivo PET imaging using nanostructured materials. With this goal in mind, we sought to synthesize fluorine-18-containing nanoparticles by mimicking well-known small molecule chemistry. Many fluorine-18-containing molecular imaging agents rely on nucleophilic displacement of a sulfonate ester by the nucleophilic fluoride-18 anion.[11] These reactions are typically run in acetonitrile, using kryptofix-222 to bind potassium. In our nanoparticle design, we chose to incorporate sulfonate esters to take advantage of this well-developed chemistry.

Our long-term goals include probing the limits of the EPR effect and determining the optimal nanoparticle size for tumor targeting. To this end, we selected amphiphilic block copolymers as scaffolds from which to build nanoparticles due to their predictable self-assembly behavior in forming micelles, the well-defined nature of such nanostructures, and the ability to control micelle size by modifying block lengths and ratios.[12] Ring opening metathesis

Scheme 1. Monomer Syntheses[a]
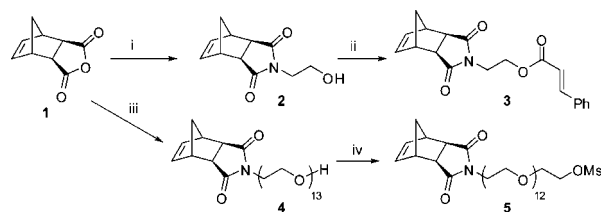
[a] Reaction conditions: (i) H₂NCH₂CH₂OH, NEt₃, toluene, DS-trap; (ii) *trans*-cinnamic acid, EDC, DMAP, CH₂Cl₂, rt; (iii) H₂N(CH₂CH₂O)₁₃OH, C₆H₆, DS-trap; (iv) MsCl, NEt₃, −30 °C.

polymerization (ROMP) provides a method for producing very low polydispersity amphiphilic block copolymers without protecting group chemistry.[13] This is a distinct advantage over other living polymerization techniques, such as anionic polymerization and controlled free radical polymerization. Syntheses of nanoparticles using these techniques typically require multiple polymerization steps, followed by one or more deprotection or functionalization reactions. Many of the steps performed after polymerization require lengthy purification procedures such as dialysis. Additionally, living ROMP using substituted norbornenes produces polymers whose degrees of polymerization can be easily and precisely controlled by adjusting the monomer to catalyst ratio.[14] When polymerizing substituted norbornenes, ROMP is free of chain transfer and termination events. Reactions are therefore typically run to complete conversion, allowing for extremely precise control over polymer molecular weight. As a result, factors affecting nanoparticle size and shape, such as the length and relative ratio of the hydrophilic and hydrophobic blocks, can be easily modified to produce a wide variety of nanoparticle architectures in a short amount of time. We show here that cross-linked micelles can be easily synthesized and efficiently functionalized with fluorine-18 using amphiphilic block copolymers made by ROMP.

The synthesis of nanoparticles containing functional groups for cross-linking, biocompatibility, and facile radiofluorination required the development of block copolymers that exhibited all of these elements. Substituted exo-norbornenes were chosen as the monomers due to their ability to undergo living ROMP, as well as their ability to be easily functionalized. Specifically, norbornene-imides were used because the condensation of exo-anhydride **1** with functionalized amines is a versatile reaction capable of forming a variety of monomers (Scheme 1).

As the cross-linking element, we chose the cinnamoyl group because it has been used previously as a photo-cross-linker in nanoparticle syntheses.[15] Cross-linking of the micelles is necessary to ensure that the nanoparticles stay intact upon dilution in the bloodstream, as the polymer concentration can drop below the critical micelle concentration (cmc) in vivo. Under irradiation with ultraviolet light, the *trans*-olefin of the cinnamoyl group undergoes
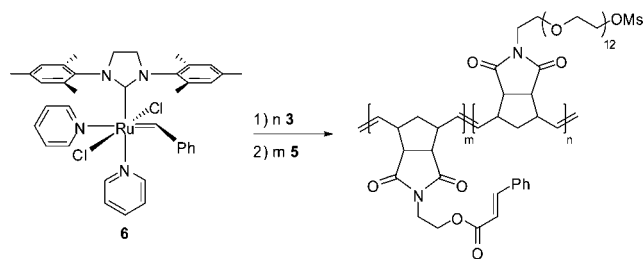
Scheme 2. Polymer Synthesis

Table 1. GPC Characterization of Block Copolymers

entry	m	n	M_n (theo)	M_n (GPC)	PDI
1	50	150	140400	133200	1.01
2	100	300	280500	280000	1.03
3	200	600	560100	544000	1.18
4	400	1200	1124000	1222000	1.73

Table 2. Characterization of Nanoparticles

entry	polymer M_n	diameter (AFM)	diameter (DLS)
1	133200	12.7 ± 2.6 nm	47.4 ± 7.5 nm
2	280000	16.4 ± 4.5 nm	58.1 ± 1.8 nm
3	544000	21.1 ± 3.9 nm	79.7 ± 9.7 nm
4	1222000	39.7 ± 4.0 nm	142.5 ± 6.8 nm

Scheme 3. Fluorinated Nanoparticle Synthesis[a]

[a] Black lines represent polymer backbone; blue lines and red lines represent pendent PEG and cinnamoyl groups, respectively. Purple balls represent mesylate groups, and green balls represent fluorine atoms. Conditions: (i) dialysis against H_2O; (ii) $h\nu$, 3 min; (iii) (1) $K^{18}F$, kryptofix-222, K_2CO_3, BHT, MeCN, 120 °C, 60 min; (2) $K^{19}F$, kryptofix-222, MeCN, 80 °C, 30 min.

a [2 + 2] dimerization to afford a tetrasubstituted cyclobutane ring.[16] Hydrophobic monomer **3** was synthesized by reaction of exo-norbornene anhydride **1** with aminoethanol to produce norbornene-imide **2**, followed by coupling with *trans*-cinnamic acid using EDC.

We chose to incorporate PEG into the hydrophilic monomer because PEG is known to be nonimmunogenic and nontoxic, and both linear and grafted PEG chains are known to provide a stealth coating for nanoparticles in the bloodsteam.[17] Mesylate leaving groups were added to the end of the PEG chain for later displacement by radioactive fluoride. The mesylate group was preferred after examination of a variety of leaving groups due to its high stability and solubility. The PEGylated norbornene imide **4** was synthesized by reaction of a previously reported monoaminated poly(ethylene glycol) (PEG) chain with exo-norbornene anhydride **1**, followed by reaction with mesyl chloride to produce hydrophilic monomer **5**. Many lengths of PEG chains were examined, but PEG600 was found to provide the desired solubility while retaining high reactivity during ROMP.

To demonstrate the capability of this synthetic method in forming a broad range of nearly monodisperse nanoparticles, four different polymers of varying molecular weights were made (Scheme 2). Sequential copolymerization of the two monomers was carried out under argon on the benchtop in THF. The ruthenium olefin metathesis catalyst $(H_2IMes)(pyr)_2(Cl)_2Ru=CHPh$ (**6**) was chosen as the initiator due to its ability to produce extremely low polydispersity polymers[18] and its good benchtop stability. Polymerization of the first monomer was complete after 1–2 min, at which point the second monomer was added to the reaction mixture. All block copolymerizations were complete in 30 min. Quenching with ethyl vinyl ether and precipitation into ether/hexanes (1:1) afforded the desired products in excellent yields. The materials showed PDIs that were as low as polymers produced by other similar initiators.[14] Characterization by gel permeation chromatography (GPC) showed monomodal, very low polydispersity peaks for most of the polymers (Table 1, entries 1–3). Broadening of the PDI was observed with higher MW polymers (Table 1, entry 4). This broadening is likely

due to catalyst death. A block ratio of 3:1 hydrophilic/hydrophobic was chosen after extensive study of the solubility of nanoparticles with various block lengths.

Micelle formation was accomplished by dissolving a given polymer in THF, a good solvent for both blocks, followed by slowly adding water to the solution. The resulting micelle solution was then dialyzed against water to remove the THF (Scheme 3). The micelles were analyzed by dynamic light scattering (DLS) and atomic force microscopy (AFM) before cross-linking to ensure that no structural or significant size changes occurred during irradiation (Figure S1).

The cross-linking reaction was accomplished by irradiation of the micelles with UV light in degassed water at room temperature. The extent of the reaction was kept between 15 and 25% as longer reaction times caused the nanoparticles to become insoluble. Typically, only 3 min of irradiation was necessary to achieve this conversion. Absorption at the peak absorbance of 278 nm was measured to evaluate the extent of cross-linking. While a small amount of intrachain cross-linking is inevitable, this contribution is expected to be small due to the compact nature of the micelle core.

Characterization of the micelles and nanoparticles (Table 2) was accomplished in the solid state by AFM, as shown in Figure 1, and in solution by DLS. The expected trend of increasing nanoparticle diameter with increasing polymer molecular weight is observed, with nanoparticle diameters ranging from 12.7 to 39.7 nm by AFM and 47.4 to 142.5 nm by DLS. The apparent diameter of the nanoparticles is 2–3 times larger when measured using DLS than when measured using AFM. This effect is likely due to the swelling of the polymer chains in solution as well as the hydration sphere surrounding the particles in aqueous environments. The hydrodynamic diameter is a good indicator of the particle size in vivo. DLS measurements show that the particles fall into the desired range to effectively probe the limits of the EPR effect.[1d]

Lyophilized nanoparticle samples were used for the radiofluorination experiments. Fluoride-18 was transported in its hydrated form into the reaction vessel, and solutions of kryptofix-222, K_2CO_3, and BHT were added. The water was removed by three consecutive

n =50, m = 150   n =100, m = 300

n =200, m = 400   n =400, m = 1200
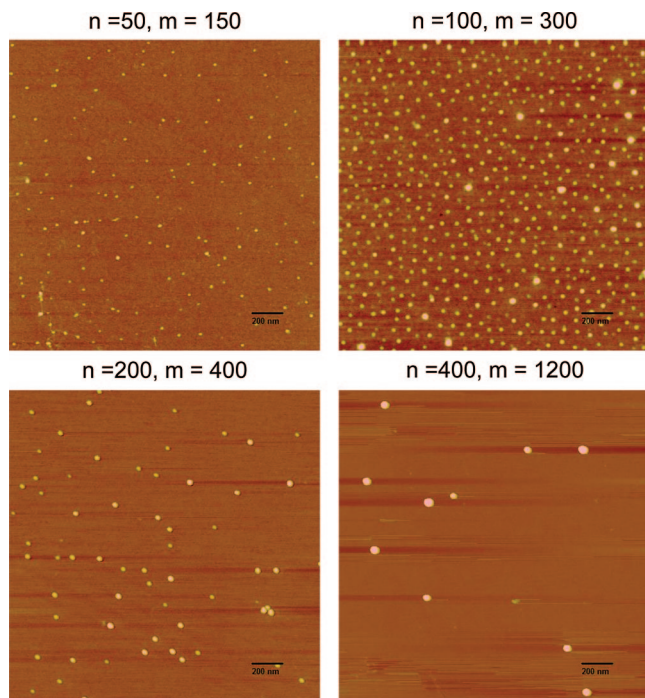
Figure 1. AFM images of nanoparticles. The nanoparticle diameters are shown to increase with increasing molecular weight of the constituent block copolymers.

additions and evaporations of acetonitrile. The nanoparticles were added as a solution in acetonitrile, and the reaction mixture was heated in a sealed vessel for 1 h at 120 °C. Because fluoride-18 is the limiting reagent, the remaining mesylates were displaced with additional fluoride-19 to avoid undesired reactions in vivo. The radiofluorinated particles were isolated by diluting the reaction mixture with water and passing this solution through neutral alumina and strongly acidic cation exchange resin. These conditions effectively removed all of the kryptofix and most of the unreacted fluoride. Measurement of the specific activity of the nanoparticles showed that 50% of the fluoride was incorporated into the product. Radiochemical purity was measured by radioTLC (Figure S2), which showed that the nanoparticles accounted for 61% of the total specific activity, meaning that 31% of the fluoride was incorporated into the nanoparticles. The bulk of the remaining activity came from unreacted fluoride. ^{1}H NMR has shown that the mesylates are completely displaced during this process.

In conclusion, fluorine-18 functionalized nanoparticles have been synthesized for use as in vivo molecular imaging agents. Block copolymer micelles were formed by the ROMP of two new, functional norbornene-based monomers. Cross-linking of the micelles yielded discrete nanoparticles that exhibited hydrodynamic diameters from 47 to 142 nm. Fluorine-18 was incorporated into the nanoparticles using standard nucleophilic fluorination chemistry in 61% radiochemical purity. Ongoing in vivo studies in mice will establish the optimal size range of nanoparticles for exploitation of the EPR effect.

References

(1) (a) Brigger, I.; Dubernet, C.; Couvreur, P. *Adv. Drug Delivery Rev.* **2002**, *54*, 631–651. (b) Sinha, R.; Kim, G. J.; Nie, S. M.; Shin, D. M. *Mol. Cancer Ther.* **2006**, *5*, 1909–1917. (c) Ferrari, M. *Nat. Rev. Cancer* **2005**, *5*, 161–171. (d) Heath, J. R.; Davis, M. E. *Annu. Rev. Med.* **2008**, *59*, 251–265.
(2) Maeda, H.; Wu, J.; Sawa, T.; Matsumura, Y.; Hori, K. *J. Controlled Release* **2000**, *65*, 271–284.
(3) (a) Lee, S. M.; Chen, H.; Dettmer, C. M.; O'Halloran, T. V.; Nguyen, S. T. *J. Am. Chem. Soc.* **2007**, *129*, 15096–15097. (b) Torchilin, V. P. *Nat. Rev. Drug Discovery* **2005**, *4*, 145–160.
(4) (a) Michalet, X.; Pinaud, F. F.; Bentolila, L. A.; Tsay, J. M.; Doose, S.; Li, J. J.; Sundaresan, G.; Wu, A. M.; Gambhir, S. S.; Weiss, S. *Science* **2005**, *307*, 538–544. (b) Smith, A. M.; Ruan, G.; Rhyner, M. N.; Nie, S. M. *Ann. Biomed. Eng.* **2006**, *34*, 3–14. (c) Bagalkot, V.; Zhang, L.; Levy-Nissenbaum, E.; Jon, S.; Kantoff, P. W.; Langer, R.; Farokhzad, O. C. *Nano Lett.* **2007**, *7*, 3065–3070.
(5) (a) Ihre, H. R.; De Jesus, O. L. P.; Szoka, F. C.; Frechet, J. M. J. *Bioconjugate Chem.* **2002**, *13*, 443–452. (b) Lee, C. C.; MacKay, J. A.; Frechet, J. M. J.; Szoka, F. C. *Nat. Biotechnol.* **2005**, *23*, 1517–1526. (c) Jain, N. K.; Asthana, A. *Exp. Opin. Drug Delivery* **2007**, *4*, 495–512.
(6) (a) Torchilin, V. P. *J. Controlled Release* **2001**, *73*, 137–172. (b) Sun, X. K.; Rossin, R.; Turner, J. L.; Becker, M. L.; Joralemon, M. J.; Welch, M. J.; Wooley, K. L. *Biomacromolecules* **2005**, *6*, 2541–2554. (c) Licciardi, M.; Giammona, G.; Du, J. Z.; Armes, S. P.; Tang, Y. Q.; Lewis, A. L. *Polymer* **2006**, *47*, 2946–2955.
(7) Heidel, J.; Mishra, S.; Davis, M. E. *Adv. Biochem. Eng. Biotechnol.* **2005**, *99*, 7–39.
(8) (a) Morawski, A. M.; Lanza, G. A.; Wickline, S. A. *Curr. Opin. Biotechnol.* **2005**, *16*, 89–92. (b) Seo, W. S.; Lee, J. H.; Sun, X. M.; Suzuki, Y.; Mann, D.; Liu, Z.; Terashima, M.; Yang, P. C.; McConnell, M. V.; Nishimura, D. G.; Dai, H. J. *Nat. Mater.* **2006**, *5*, 971–976. (c) Kobayashi, H.; Brechbiel, M. W. *Adv. Drug Delivery Rev.* **2005**, *57*, 2271–2286.
(9) Yang, Z.; Zheng, S. Y.; Harrison, W. J.; Harder, J.; Wen, X. X.; Gelovani, J. G.; Qiao, A.; Li, C. *Biomacromolecules* **2007**, *8*, 3422–3428.
(10) (a) Bartlett, D. W.; Su, H.; Hildebrandt, I. J.; Weber, W. A.; Davis, M. E. *Proc. Natl. Acad. Sci. U.S.A.* **2007**, *104*, 15549–15554. (b) Fukukawa, K.; Rossin, R.; Hagooly, A.; Pressly, E. D.; Hunt, J. N.; Messmore, B. W.; Wooley, K. L.; Welch, M. J.; Hawker, C. J. *Biomacromolecules* **2008**, *9*, 1329–1339. (c) Schipper, M. L.; Cheng, Z.; Lee, S.-W.; Bentolila, L. A.; Iyer, G.; Rao, J.; Chen, X.; Wu, A. M.; Weiss, S.; Gambhir, S. S. *J. Nucl. Med.* **2007**, *48*, 1511–1518.
(11) Lasne, M. C.; Perrio, C.; Rouden, J.; Barre, L.; Roeda, D.; Dolle, F.; Crouzel, C. *Top. Curr. Chem.* **2002**, *222*, 201–258.
(12) Stubenrauch, K.; Moitzi, C.; Fritz, G.; Glatter, O.; Trimmel, G.; Stelzer, F. *Macromolecules* **2006**, *39*, 5865–5874.
(13) (a) Bielawski, C. W.; Grubbs, R. H. *Prog. Polym. Sci.* **2007**, *32*, 1–29. (b) Maynard, H. D.; Okada, S. Y.; Grubbs, R. H. *Macromolecules* **2000**, *33*, 6239–6248. (c) Rawat, M.; Gama, C. I.; Matson, J. B.; Hsieh-Wilson, L. C. *J. Am. Chem. Soc.* **2008**, *130*, 2959–2961.
(14) Choi, T. L.; Grubbs, R. H. *Angew. Chem., Int. Ed.* **2003**, *42*, 1743–1746.
(15) Henselwood, F.; Liu, G. J. *Macromolecules* **1997**, *30*, 488–493.
(16) Khan, M.; Brunklaus, G.; Enkelmann, V.; Spiess, H. W. *J. Am. Chem. Soc.* **2008**, *130*, 1741–1748.
(17) Gref, R.; Minamitake, Y.; Peracchia, M. T.; Trubetskoy, V.; Torchilin, V. P.; Langer, R. *Science* **1994**, *263*, 1600–1603.
(18) (a) Camm, K. D.; Castro, N. M.; Liu, Y. W.; Czechura, P.; Snelgrove, J. L.; Fogg, D. E. *J. Am. Chem. Soc.* **2007**, *129*, 4168–4169. (b) Slugovc, C.; Demel, S.; Stelzer, F. *Chem. Commun.* **2002**, 2572–2573.

JA802010D